ISSN 1392-1207. MECHANIKA. Vol. 31, No. 5, 2025: 505–516

Mechanical Behaviour Analysis of Bio-Inspired Joints with Notched Flexure Hinges

Jingjing LIANG*, Ruiqin LI, Wenxiao GUO***, Lei ZHANG*, Qisheng ZHANG***
*School of Mechanical Engineering, North University of China, Taiyuan, 030051 China
**School of Mechanical Engineering, North University of China, Taiyuan, 030051 China,
E-mail: liruiqin@nuc.edu.cn (Corresponding Author)
***CCTEG Taiyuan Research Institute Co. Ltd., China, E-mail: gwx041202@163.com
https://doi.org/10.5755/j02.mech.41779

1. Introduction

Compared with traditional rigid mechanisms, flexible mechanisms utilize the elastic deformation of materials to transmit or convert motion, force, or energy. They can be fabricated as a whole, with advantages such as compact structure, no need for lubrication, frictionless operation, smooth motion, and higher precision [1-2]. With the continuous increase in demand in industrial, medical, and other fields, there is a growing requirement for higher precision in mechanisms. Consequently, flexible mechanisms are increasingly applied in robotics, bionic engineering, precision instruments, and related domains [3-4]. Due to their elasticity and capability to store and release energy through deformation, these mechanisms can be employed to mimic the flexibility of biological organisms [5], such as joints, legs, wings, and other structures, enabling corresponding motion and power transmission to achieve biomimetic effects [6-10]. This has now become a major research focus in robotics.

Domestic and foreign scholars have conducted applied studies on flexible mechanisms. Xi et al. [11] designed a bionic flexible robotic hand that employs motor-driven push rods to deform a silicone membrane, enabling adaptive grasping by wrapping around targets. Yu et al. [12] developed a slotted thin-walled flexure hinge to replace traditional revolute pair in a 3-DOF parallel robot. Meng et al. [13] designed a serial-type bionic exoskeleton robotic hand using these hinges. This device can output grasping forces sufficient for daily activities, maintain normal joint mobility, and assist in rehabilitation training and functional recovery for patients with hand dysfunction. Ma [14] proposed a novel two-finger robotic hand structure driven by pneumatic artificial muscles, which independently actuate metacarpophalangeal and interphalangeal joints through tendon cables and pulleys to transmit motion. Wang [15] developed a high-rebound elastomeric joint underactuated robotic hand. Driven by tendons, this gripper achieves adaptable grasping with strong object compatibility, while maintaining simplicity. Zhou [16] proposed a flexible robotic hand design featuring three flexible bending biomimetic joint structure (each composed of two elliptical pneumatic chambers) and a passively adaptive palm. It reliably grips both small objects and large convex-shaped targets. Liu [17] developed a pneumatic artificial muscle and created two types of flexible joints: a pneumatic multi-directional bending joint and a shaftless multi-hinge unidirectional bending joint. Wu et al. [18] designed a pneumatic soft gripper with an intra-joint skeletal structure, decoupling actuation, and force-bearing functions. Soft actuation is achieved through pneumatic chambers embedded in fibre-constrained multilayer rubber, while grasping forces are transmitted via rigid internal skeletal biomimetic joint structure. Alici et al. [19] developed a model to analyse the quasi-static bending angles of flexible pneumatic actuators fabricated from two elastomeric silicones (transparent soft silicone and discrete cavity structures). The model accurately predicts bending behaviors of such actuators. Abondance [20] created a flexible hand with two parallel pneumatic bellow-type actuators, enabling dexterous fingertip motions. Sinatra et al. [21] proposed a nanofiber-reinforced ultra-soft robotic actuator, which demonstrated minimal harm to typical jellyfish species through laboratory-validated underwater grasping capabilities with sufficiently low contact pressure.

Flexible hinges and flexible mechanisms have been widely used in fields such as bionic robots and rehabilitation robots. Its inherent ability to withstand impact loads significantly enhances the environmental adaptability of the equipment in various operational scenarios. However, stress concentration is prone to occur at the root of the notch in notch-type flexible hinges, which affects their reliability. Further in-depth research is still needed on how the shape and size of the notch influence the performance of flexible mechanisms composed of such hinges. Additionally, the application research integrating bionics still offers vast exploration space. Therefore, based on bionic principles, such as the excellent compliance of biological joints, this paper applies notch-type flexible hinges as bionic joints to the design of flexible mechanisms and proposes a novel flexible gripping mechanism inspired by bionic joints, a study was conducted on its performance.

This paper is organized as follows. Section 2 presents a novel structure of flexible gripping mechanism. In Section 3, an analytical calculation of the output compliance of the biomimetic joint structure with notch-based flexure hinges is performed, and FEA is conducted to evaluate the compliance characteristics of three distinct notch-type configurations. In Section 4, the analytical solutions are validated through compari-

son with FEA results. Furthermore, the influence of structure parameters on the performance of bionic joint linkage mechanism is investigated, and the compliance properties of the three notch-type designs are systematically compared. Conclusions are drawn in Section 5.

2. Structure of Flexible Gripping Mechanism

The flexible gripping mechanism is assembled with three biomimetic joint structure with notch-based flexure hinges arranged in a 120° equidistant layout. This configuration notably enhances stability during the grasping process. The biomimetic joint structure with notch-based flexure hinges is driven by cylinder-actuated bending mechanisms to achieve bending deformation, enabling effective object grasping through bio-inspired motion imitation. Fig.1, a illustrates the integrated structural model of flexible gripping mechanism. The biomimetic joint structure is fabricated from polypropylene and incorporate notch-type flexure bionic joints, demonstrating exceptional flexibility and adaptability. Given that the grasping function of the flexible manipulator primarily relies on the bending deformation of the biomimetic joint structure, the design analysis of the biomimetic joint structure with notch-based flexure hinges is critical. The specific structure form of the flexible gripping mechanism is shown in Table 1, while the models of bionic joint linkage mechanism with triple notched flexure configurations are depicted in Fig. 1, b.

Table 1

Structure forms of the flexible gripping mechanism

Driving mode	Cylinder drive
Layout form	Equidistant layout
Palm connection	fixed joint
Number of biomimetic joint structure	three biomimetic joint structure
Bionic joint form	U-shaped flexure hinge
	Arc-shaped flexure hinge
	Elliptical arc-shaped flexure hinge
Material Composition	Polypropylene (Young's modulus 2, Poisson's ratio 4.5)

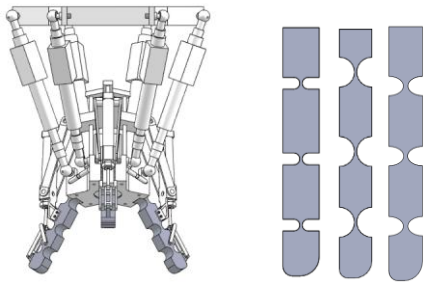

a b

Fig. 1 Flexible gripping mechanism model: a – an integrated structural model of flexible gripping mechanism, b – models of bionic joint linkage mechanism with triple notched flexure configurations

3. Analytical Calculation of the Compliance for Bionic Joint Linkage Mechanism

The bionic joint linkage mechanism can be modelled as 3-RRR flexible link, as depicted in Fig. 2. For 3-RRR flexible link, a coordinate system origin is established at point O, the total flexibility of the flexible link at point O is the summation of the flexibilities of each individual flexure hinge acting in the same direction. The variables Δx, Δy, and $\Delta\alpha$ represent the displacements of the flexible link along x-axis and y-axis, as well as the rotation angle around z-axis, respectively. $C\Delta x$, $C\Delta y$ and $C\Delta\alpha$ represent the linear compliance of the flexible link along x-axis and y-axis, as well as the angular compliance around z-axis, respectively. $\Delta x_{i,F_x}$, $\Delta x_{i,F_y}$, $\Delta x_{i,M_z}$, $\Delta y_{i,F_x}$, $\Delta y_{i,F_y}$, $\Delta y_{i,M_z}$, $\Delta\alpha_{i,F_x}$, $\Delta\alpha_{i,F_y}$, $\Delta\alpha_{i,M_z}$ represent the linear displacements and angular displacements, respectively, generated at point O due to the hinge's compliance when external forces and moments are applied. The compliance of the i-th hinge is respectively represented by $\Delta x_i / F_x$, $\Delta y_i / F_y$ and $\Delta\alpha_i / M_z$. Taking the U-shaped flexure hinge as an example, the compliance matrix of 3-RRR flexible link is systematically derived.

The compliance matrix of 3-RRR flexible link at point O, caused by the first flexure hinge, can be expressed as

$$\boldsymbol{C} = \begin{bmatrix} C\Delta x_{1,F_x} & C\Delta x_{1,F_y} & C\Delta x_{1,M_z} \\ C\Delta y_{1,F_x} & C\Delta y_{1,F_y} & C\Delta y_{1,M_z} \\ C\Delta\alpha_{1,F_x} & C\Delta\alpha_{1,F_y} & C\Delta\alpha_{1,M_z} \end{bmatrix}. \quad (1)$$

The angular compliance of 3-RRR flexible link about z-axis, induced by the deformation of the first flexure hinge, can be expressed as follows:

The angular compliance generated by the force $\boldsymbol{F}_x$

$$C\Delta\alpha_{1,F_x} = -C_{\alpha_z - M_z} \cdot \left(l_1 + l_2 + l_3 + 5r\right). \quad (2)$$

The angular compliance generated by the force $\boldsymbol{F}_y$

$$C\Delta\alpha_{1,F_y} = 0. \quad (3)$$

The angular compliance generated by the torque $\boldsymbol{M}_z$

$$C\Delta\alpha_{1,M_z} = \left[C_{\alpha_z - M_z}\right]_1 = \left[\frac{\Delta\alpha_1}{M_z}\right]. \quad (4)$$

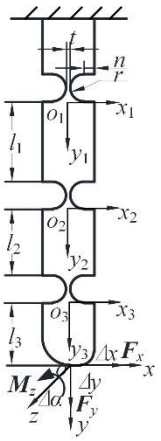

Fig. 2 Structure parameters and load distribution of 3-RRR flexible link

The linear compliance along *y*-axis of 3-RRR flexible link generated by the first flexure hinge. The linear compliance along *y*-axis is induced by the force $\boldsymbol{F}_x$

$$C\Delta y_{1,F_x} = \frac{\Delta\alpha_{1,F_x}\cdot(l_1+l_2+l_3+4r)+\Delta y_{1,F_x}}{F_x} = \\ = C\Delta\alpha_{1,F_x}\cdot(l_1+l_2+l_3+4r)+C\Delta y_{1,F_x} = \\ = -\left[C_{\alpha_z-M_z}\right]_1\cdot(l_1+l_2+l_3+4r)\cdot(l_1+l_2+l_3+5r)- \\ -\left[C_{y-F_y}\right]_1. \quad (5)$$

The linear compliance along *y*-axis is induced by the force $\boldsymbol{F}_y$

$$C\Delta y_{1,F_y} = 0. \quad (6)$$

The linear compliance along *y*-axis is induced by the Torque $\boldsymbol{M}_z$

$$C\Delta y_{1,M_z} = C_{\alpha_z-M_z}(l_1+l_2+l_3+3r). \quad (7)$$

The linear compliance along *x*-axis of 3-RRR flexible link generated by the first flexure hinge:

The linear compliance along *x*-axis is induced by the force $\boldsymbol{F}_x$

$$C\Delta x_{1,F_x} = \left(C_{x-F_x}\right)_1. \quad (8)$$

The linear compliance along *x*-axis is induced by the force $\boldsymbol{F}_y$

$$C\Delta x_{1,F_y} = 0. \quad (9)$$

The linear compliance along *x*-axis is induced by the torque $\boldsymbol{M}_z$

$$C\Delta x_{1,M_z} = 0. \quad (10)$$

When a force or torque is applied, the displacement at point *O* of 3-RRR flexible link, caused by the first flexure hinge, can be expressed as:

$$\begin{bmatrix}\Delta x_1 & \Delta y_1 & \Delta\alpha_1\end{bmatrix}^T = \boldsymbol{C}_1\times\boldsymbol{F}_O. \quad (11)$$

$$\boldsymbol{C}_1 = \begin{bmatrix} \left(C_{x-F_x}\right)_1 & 0 & 0 \\ -\left[C_{\alpha_z-M_z}\right]_1\cdot(l_1+l_2+l_3+4r)\cdot(l_1+l_2+l_3+5r)-\left[C_{y-F_y}\right]_1 & 0 & C_{\alpha_z-M_z}(l_1+l_2+l_3+3r) \\ -C_{\alpha_z-M_z}\cdot(l_1+l_2+l_3+5r) & 0 & C\Delta\alpha_{z,M_z} \end{bmatrix}. \quad (12)$$

The compliance matrix of 3-RRR flexible link at point *O*, caused by the second flexure hinge, can be expressed as

$$\boldsymbol{C} = \begin{bmatrix} C\Delta x_{2,F_x} & C\Delta x_{2,F_y} & C\Delta x_{2,M_z} \\ C\Delta y_{2,F_x} & C\Delta y_{2,F_y} & C\Delta y_{2,M_z} \\ C\Delta\alpha_{2,F_x} & C\Delta\alpha_{2,F_y} & C\Delta\alpha_{2,M_z} \end{bmatrix}. \quad (13)$$

The angular compliance of 3-RRR flexible link about *z*-axis, induced by the deformation of the second flexure hinge, can be expressed as follows.

The angular compliance generated by the force $\boldsymbol{F}_x$

$$C\Delta\alpha_{2,F_x} = -C_{\alpha_z-M_z}\cdot(l_2+l_3+3r). \quad (14)$$

The angular compliance generated by the force $\boldsymbol{F}_y$

$$C\Delta\alpha_{2,F_y} = 0. \quad (15)$$

The angular compliance generated by the torque $\boldsymbol{M}_z$

$$C\Delta\alpha_{2,M_z} = \left(C_{\alpha_z-M_z}\right)_2. \quad (16)$$

The linear compliance along *y*-axis of 3-RRR flexible link generated by the second flexure hinge.

The linear compliance along *y*-axis is induced by the force $\boldsymbol{F}_x$

$$C\Delta y_{2,F_x} = \frac{\Delta\alpha_{2,F_x}\cdot(l_2+l_3+2r)+\Delta y_{2,F_x}}{F_x} = \\ = C\Delta\alpha_{2,F_x}\cdot(l_2+l_3+2r)+C\Delta y_{2,F_x} = \\ = -\left(C_{\alpha_z-M_z}\right)_2\cdot(l_2+l_3+2r)\cdot(l_2+l_3+3r)-\left(C_{y-F_y}\right)_2. \quad (17)$$

The linear compliance along *y* -axis is induced by the force $\boldsymbol{F}_y$

$$C\Delta\alpha_{2,F_y} = 0. \quad (18)$$

The linear compliance along *y*-axis is induced by the torque $\boldsymbol{M}_z$

$$C\Delta y_{2,M_z} = \left(C_{\alpha_z - M_z}\right)_2 \left(l_2 + l_3 + 3r\right). \tag{19}$$

The linear compliance along *x*-axis of 3-RRR flexible link generated by the second flexure hinge:

The linear compliance along *x*-axis is induced by the force $\boldsymbol{F}_x$

$$C\Delta x_{2,F_x} = \left(C_{x-F_x}\right)_2. \tag{20}$$

The linear compliance along *x* -axis is induced by the force $\boldsymbol{F}_y$

$$C\Delta x_{2,F_y} = 0. \tag{21}$$

The linear compliance along *x*-axis is induced by the torque $\boldsymbol{M}_z$

$$C\Delta x_{2,M_z} = 0. \tag{22}$$

When a force or torque is applied, the displacement at point *O* of 3-RRR flexible link, caused by the second flexure hinge, can be expressed as:

$$\begin{bmatrix}\Delta x_2 & \Delta y_2 & \Delta\alpha_2\end{bmatrix}^T = C_2 \times F_O, \tag{23}$$

$$\boldsymbol{C}_2 = \begin{bmatrix} \left(C_{x-F_x}\right)_2 & 0 & 0 \\ -\left(C_{\alpha_z - M_z}\right)_2 \cdot \left(l_2 + l_3 + 2r\right) \cdot \left(l_2 + l_3 + 3r\right) - \left(C_{y-F_y}\right)_2 & 0 & \left(C_{\alpha_z - M_z}\right)_2 \left(l_2 + l_3 + 3r\right) \\ -C_{\alpha_z - M_z} \cdot \left(l_2 + l_3 + 3r\right) & 0 & \left(C_{\alpha_z - M_z}\right)_2 \end{bmatrix}. \tag{24}$$

The compliance matrix of 3-RRR flexible link at point *O*, caused by the third flexure hinge, can be expressed as

$$\boldsymbol{C} = \begin{bmatrix} C\Delta x_{3,F_x} & C\Delta x_{3,F_y} & C\Delta x_{3,M_z} \\ C\Delta y_{3,F_x} & C\Delta y_{3,F_y} & C\Delta y_{3,M_z} \\ C\Delta\alpha_{3,F_x} & C\Delta\alpha_{3,F_y} & C\Delta\alpha_{3,M_z} \end{bmatrix}. \tag{25}$$

The angular compliance of 3-RRR flexible link about *z*-axis, induced by the deformation of the third flexure hinge, can be expressed as follows:

The angular compliance generated by force $\boldsymbol{F}_x$

$$C\Delta\alpha_{3,F_x} = -C_{\alpha_z - M_z} \cdot \left(l_3 + r\right). \tag{26}$$

The angular compliance generated by force $\boldsymbol{F}_y$

$$C\Delta\alpha_{3,F_y} = 0. \tag{27}$$

The angular compliance generated by the torque $\boldsymbol{M}_z$

$$C\Delta\alpha_{3,M_z} = \left(C_{\alpha_z - M_z}\right)_3. \tag{28}$$

The linear compliance along *y*-axis of 3-RRR flexible link generated by the third flexure hinge:

The linear compliance along *y*-axis is induced by the force $\boldsymbol{F}_x$

$$C_\Delta y_{3,F_x} = \frac{\Delta\alpha_{3,F_x} \cdot l_3 + \Delta y_{3,F_x}}{F_x} = C\Delta\alpha_{3,F_x} \cdot l_3 + C_\Delta y_{3,F_x} = \\ = -\left(C_{\alpha_z - M_z}\right)_3 \cdot l_3 (l_3 + 2r) - \left(C_{y-F_y}\right)_3. \tag{29}$$

The linear compliance along *y*-axis is induced by the force $\boldsymbol{F}_y$

$$C\Delta y_{3,F_y} = 0. \tag{30}$$

The linear compliance along *y* -axis is induced by the torque $\boldsymbol{M}_z$

$$C\Delta y_{3,M_z} = \left(C_{\alpha_z - M_z}\right)_3 \left(l_3 + r\right). \tag{31}$$

The linear compliance along *x*-axis of 3-RRR flexible link generated by the third flexure hinge:

The linear compliance along *x*-axis is induced by the force $\boldsymbol{F}_x$

$$C\Delta x_{3,F_x} = \left(C_{x-F_x}\right)_3. \tag{32}$$

The linear compliance along *x*-axis is induced by the force $\boldsymbol{F}_y$

$$C\Delta x_{3,F_y} = 0. \tag{33}$$

The linear compliance along the *x*-axis is induced by the torque $\boldsymbol{M}_z$

$$C\Delta x_{3,M_z} = 0. \tag{34}$$

When a force or torque is applied, the displacement at point *O* of 3-RRR flexible link, caused by the third flexure hinge, can be expressed as

$$\begin{bmatrix}\Delta x_3 & \Delta y_3 & \Delta\alpha_3\end{bmatrix}^T = \boldsymbol{C}_3 \times \boldsymbol{F}_O. \tag{35}$$

$$\boldsymbol{C}_3 = \begin{bmatrix} \left(C_{x-F_x}\right)_3 & 0 & 0 \\ -\left(C_{\alpha_z-M_z}\right)_3 \cdot l_3\left(l_3+2r\right)-\left(C_{y-F_y}\right)_3 & 0 & \left(C_{\alpha_z-M_z}\right)_3\left(l_3+r\right) \\ -C_{\alpha_z-M_z}\cdot\left(l_3+r\right) & 0 & \left(C_{\alpha_z-M_z}\right)_3 \end{bmatrix}. \tag{36}$$

The output compliance matrix of 3-RRR flexible link at point O is the sum of three individual compliance matrices C_1, C_2, and C_3

$$\boldsymbol{C}_{RRR,O} = \boldsymbol{C}_1 + \boldsymbol{C}_2 + \boldsymbol{C}_3 . \tag{37}$$

Because the structure dimensions of flexure hinges 1, 2, and 3 are identical, it follows that

$$C_{RRR,O} = \begin{bmatrix} 3C_{x-F_x} & 0 & 0 \\ -C_{\alpha_z-M_z}\cdot\left[\left(\sum_{i=1}^{3} l_i+4r\right)\cdot\left(\sum_{i=1}^{3} l_i+5r\right)+\left(\sum_{i=1}^{2} l_i+2r\right)\cdot\left(\sum_{i=1}^{3} l_i+3r\right)+l_3\left(l_3+2r\right)\right]-3C_{y-F_y} & 0 & C_{\alpha_z-M_z}\cdot\left(l_1+2l_2+3l_3+7r\right) \\ -C_{\alpha_z-M_z}\cdot\left(l_1+2l_2+3l_3+9r\right) & 0 & 3C_{\alpha_z-M_z} \end{bmatrix}. \tag{38}$$

4. Finite Element Analysis of the Compliance Characteristics of Flexible Link

4.1. Modelling and compliance analysis of 3-RRR flexible link

In order to verify the compliance matrix of the derived 3-RRR flexible link, the compliance of 3-RRR flexible link structure based on three different notch types of flexure hinge joints was analyzed by finite element method [22]. Each of the three flexure hinge joints in each 3-RRR flexible link has the same structure. The three types are U-shaped flexure hinge, circular arc-shaped flexure hinge and elliptical arc-shaped flexure hinge. Nine models in three groups were selected for analysis, and their structure parameters are shown in Table 2. As shown in Fig. 3, the upper end was fixed, and a unit load was applied at the symmetrical center "*O*" point of the distal phalanx at the lower end:

$$F_x = F_y = 1\,\mathrm{N}, \quad M_z = 1\,\mathrm{N}\cdot\mathrm{m}. \tag{39}$$

The finite element results were obtained by analyzing three types of 3-RRR flexible links. A comparison between the analytical solutions and the finite element solutions for these three types of 3-RRR flexible links is presented in Table 3, where "A" denotes the analytical solution and "F" denotes the finite element solution. The errors between the two methods for all cases are less than 8.1%.

4.2. Influences of the parameters of notch size on the compliance, stress and strain

For the flexible coupling mechanism of the bionic joints with three types of hinges, without loss of generality, we assume that two parameters pertaining to notch sizes

Fig. 3 Finite element mesh model of 3-RRR flexible link

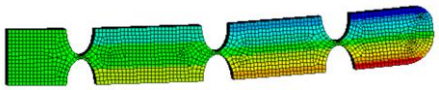

Fig. 4 Bending deformation analysis model of 3-RRR flexible link finite element

are variable while the remaining parameters are held constant. The structural dimensions of the flexure link are specified as L = 116 mm and W = 15 mm. For 3-RRR flexible linkage mechanism with U-shaped flexure hinges, when n is held constant, r and t are variables that vary within their ranges $n \in [3.75, 6]$, $t \in [1, 5.5]$. Then, the relationships between the compliance, stress, and strain of the U-shaped flexure hinge and the parameters of notch sizes r and t are plotted using ANSYS and MATLAB, as shown in Fig. 5, a-e. From these plots, several characteristics can be observed, as described below.

As illustrated in Fig. 5, a-e, the compliance, stress, and strain of the U-shaped notch exhibit nonlinear increases as the radius r of the arc section grows. Conversely, these parameters decrease nonlinearly with an increase in the minimum thickness t. The effect of the arc radius r on compliance, stress, and strain is more pronounced compared to that of the minimum thickness t. Within the range of values for r and t, there exist both maximum and minimum values for the various compliance. When r assumes its minimum value and t reaches its maximum value, both compliance and stress and strain attain their minimum values.

For 3-RRR flexible linkage mechanism with U-shaped flexure hinges. When r is held constant, n and t are variables that vary within their ranges $n \in [2.75, 5]$, $t \in [1, 5.5]$. Then, the relationships between the compliance, stress, and strain of the U-shaped flexure hinge and the parameters of notch sizes n and t are plotted using ANSYS and MATLAB, as shown in Fig. 6, a-e. From these plots, several characteristics can be observed, as described below.

Table 2

Structure parameters of 3-RRR flexible link with three distinct types of notches

Parameters / Type of hinge	n, mm	r, mm	t, mm	a, mm	b, mm	l_1, mm	l_2, mm	l_3, mm
Circular flexure hinge		7	1	/	/	23	19	19
		6	3					
		5	5					
U-shaped flexure hinge	2	5	1	/	/	27	23	21
	1	5	3					
	3	2	5					
Elliptical arc flexure hinge			1	7	4	29	25	22
			2	6.5	5			
			3	6	6			

Table 3

Comparison between analytical and finite element results for the compliance factors

Type of hinge	Types of solution and error	C_{x-F_x}, m/N	C_{y-F_y}, m/N	$C_{\alpha_z-M_z}$, rad/N•m
Circular flexure hinge	A	3.28×10^{-2}	28.4×10^{-2}	1.52×10^{-3}
	F	3.35×10^{-2}	27.3×10^{-2}	1.41×10^{-3}
	Error /(%)	2.1	4.03	7.8
	A	2.46×10^{-3}	16.13×10^{-3}	0.037×10^{-3}
	F	2.35×10^{-3}	16.99×10^{-3}	0.04×10^{-3}
	Error /(%)	4.5	5.3	8.1
	A	0.76×10^{-3}	5.24×10^{-3}	0.024×10^{-3}
	F	0.704×10^{-3}	5.135×10^{-3}	0.023×10^{-3}
	Error /(%)	7.3	2	4.2
U-shaped flexure hinge	A	2.92×10^{-2}	22.7×10^{-2}	1.31×10^{-3}
	F	2.86×10^{-2}	23.3×10^{-2}	1.24×10^{-3}
	Error /(%)	2.1	2.58	5.65
	A	2.16×10^{-3}	15.21×10^{-3}	0.023×10^{-3}
	F	2.19×10^{-3}	15.63×10^{-3}	0.022×10^{-3}
	Error /(%)	1.4	2.8	4.3
	A	0.71×10^{-3}	4.48×10^{-3}	0.025×10^{-3}
	F	0.66×10^{-3}	4.63×10^{-3}	0.023×10^{-3}
	Error /(%)	7	3.4	8
Elliptical arc flexure hinge	A	2.68×10^{-2}	23.5×10^{-2}	1.31×10^{-3}
	F	2.77×10^{-2}	22.4×10^{-2}	1.4×10^{-3}
	Error /(%)	3.25	4.91	6.9
	A	5.59×10^{-3}	38.72×10^{-3}	0.072×10^{-3}
	F	5.76×10^{-3}	39.67×10^{-3}	0.068×10^{-3}
	Error /(%)	3.04	2.45	5.6
	A	2.56×10^{-3}	15.98×10^{-3}	0.039×10^{-3}
	F	2.45×10^{-3}	17.03×10^{-3}	0.042×10^{-3}
	Error /(%)	4.3	6.57	7.7

As illustrated in Fig. 6, a-e, the compliance, stress, and strain exhibit nonlinear increases as the depth n of the straight-line segment of the U-shaped notch grows. Conversely, these parameters decrease nonlinearly with an increase in the minimum thickness t. The influence of n on compliance, stress, and strain becomes more pronounced when t is relatively small. Within the range of values for n and t, there exist both maximum and minimum values for flexibility. The minimum values for compliance, stress and strain occur when r is at its smallest and t is at its largest. For 3-RRR flexible linkage mechanism with U-shaped flexure hinges, when t is held constant, n and r are variables that vary within their ranges $n \in [1, 5.5]$, $r \in [1.5, 6]$. Then, the relationships between the compliance, stress, and strain of the U-shaped flexure hinge and the parameters of notch sizes n and r are plotted using ANSYS and MATLAB, as shown in Fig. 7, a-e. From these plots, several characteristics can be observed, as described below.

As illustrated in Fig. 7, a-e, as the depth n of the straight-line segment of the U-shaped notch increases, both compliance C_{x-F_x}, C_{y-F_y} exhibit linear decreases. Conversely, compliance $C_{\alpha_z-M_z}$ and stress decrease nonlinearly with further changes in these parameters. With increasing values of n and r, the strain initially decreases gradually, reaches a minimum value, and subsequently rises, forming pronounced nonlinear surface fluctuations. When the radius r of the arc segment of the U-shaped notch increases, compliance C_{x-F_x}, C_{y-F_y} increase linearly, whereas compliance $C_{\alpha_z-M_z}$ and stress exhibit nonlinear increases. The in-

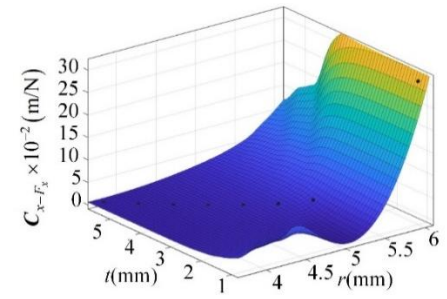

a

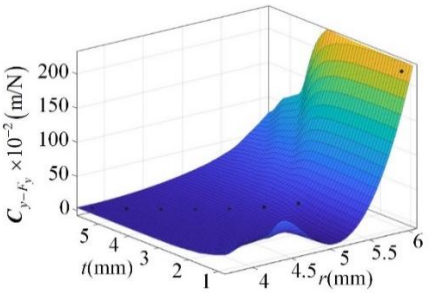

b

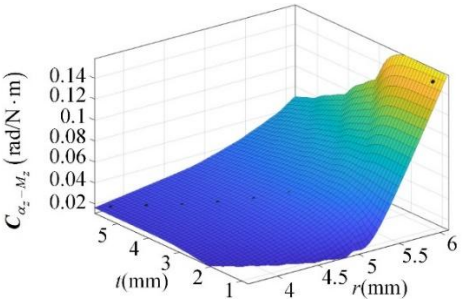

c

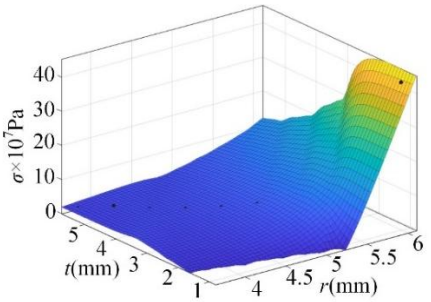

d

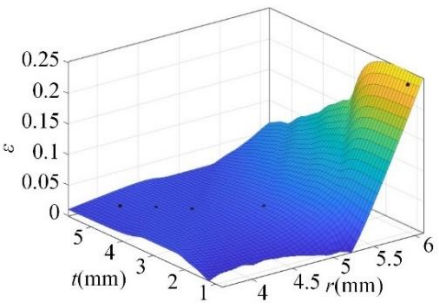

e

Fig. 5 The influence of parameters *r, t* on compliance, stress and strain: a – compliance C_{x-F_x}, b – compliance C_{y-F_y}, c – compliance $C_{\alpha z-M_z}$, d – stress; e – strain

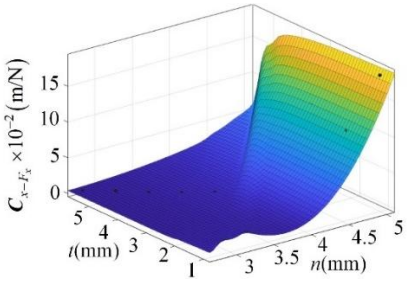

a

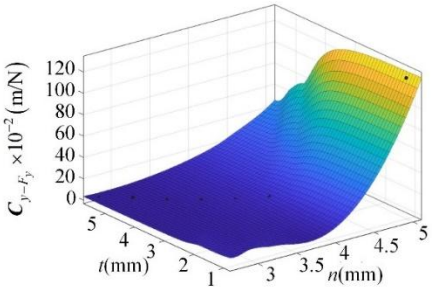

b

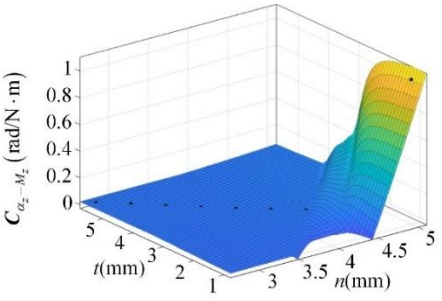

c

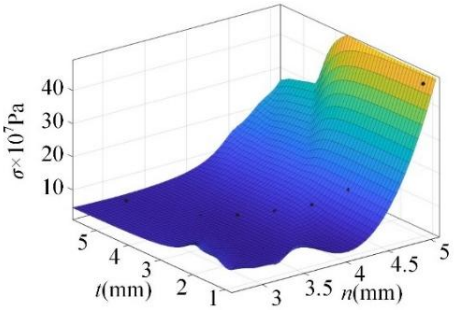

d

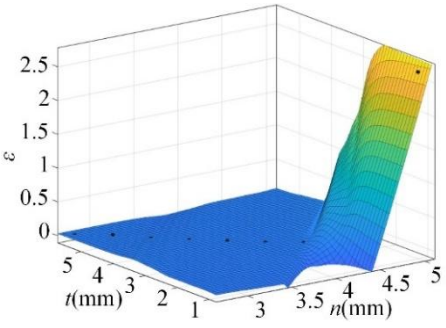

e

Fig. 6 The influence of parameters *n, t* on compliance, stress and strain: a – compliance C_{x-F_x}, b – compliance C_{y-F_y}, c – compliance $C_{\alpha_z-M_z}$, d – stress; e – strain

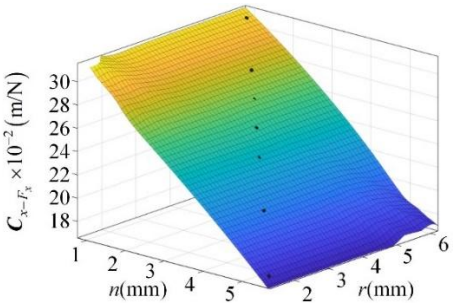

a

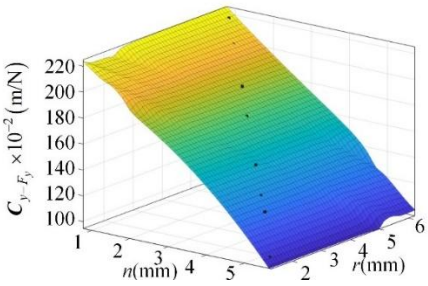

b

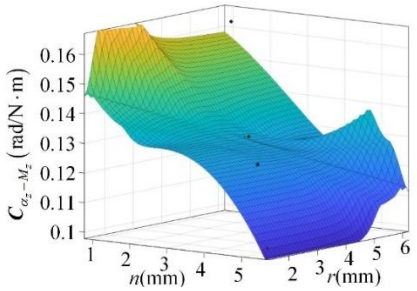

c

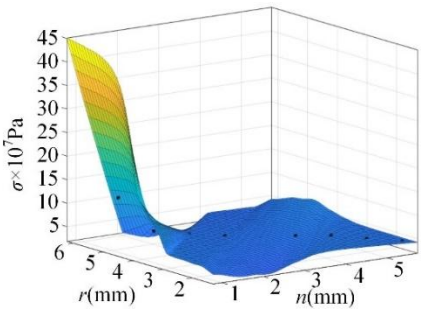

d

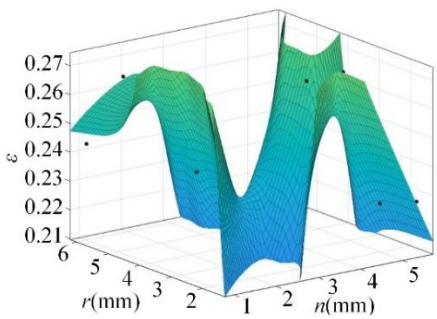

e

Fig. 7 The influence of parameters *n, r* on compliance, stress and strain: a – compliance C_{x-Fx}, b – compliance C_{y-Fy}, c – compliance $C_{\alpha z-Mz}$, d – stress, e – strain

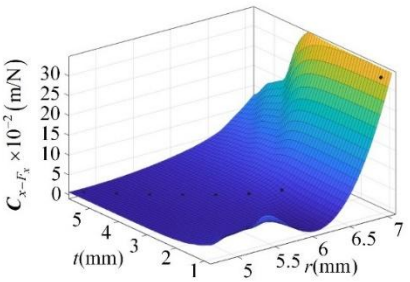

a

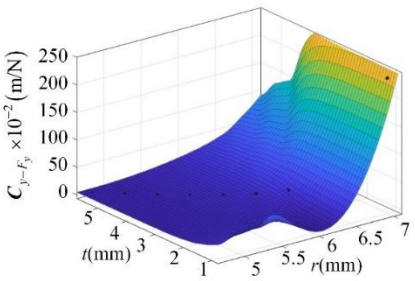

b

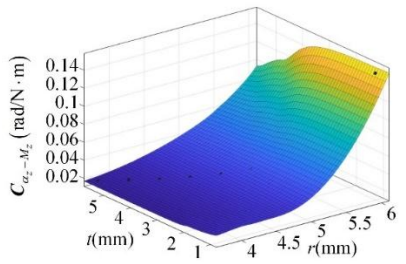

c

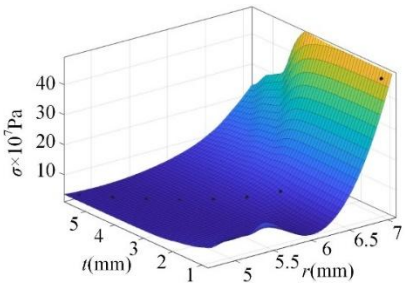

d

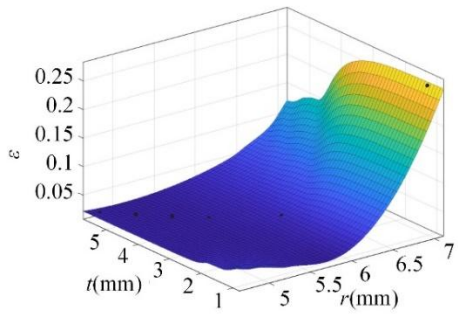

e

Fig. 8 The influence of parameters *r, t* on compliance, stress and strain: a – compliance C_{x-Fx}, b – compliance C_{y-Fy}, c – compliance $C_{\alpha z-Mz}$, d – stress; e – strain

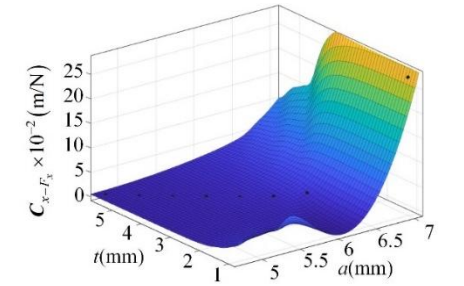

a

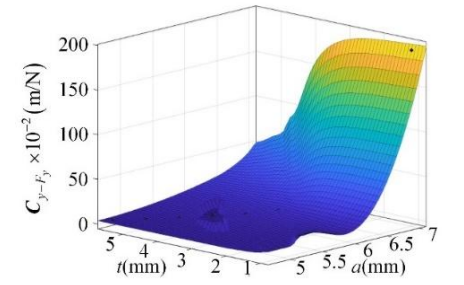

b

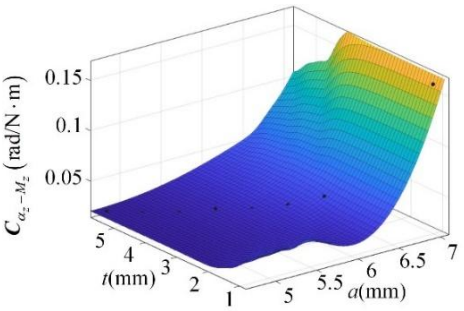

c

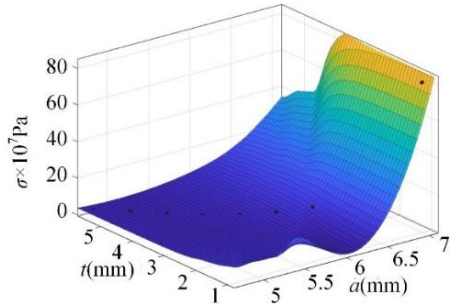

d

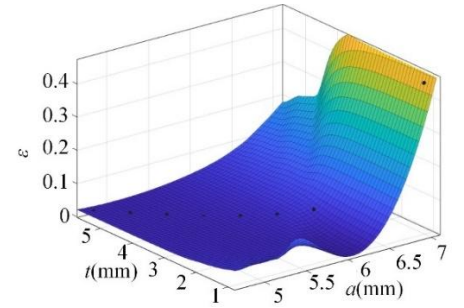

e

Fig. 9 The influence of parameters *a, t* on compliance, stress and strain: a – compliance C_{x-F_x}, b – compliance C_{y-F_y}, c – compliance $C_{\alpha_z-M_z}$, d – stress, e – strain

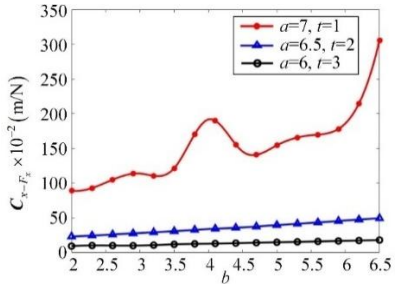

a

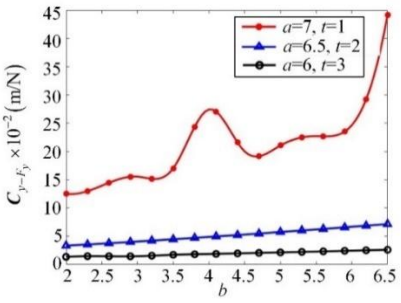

b

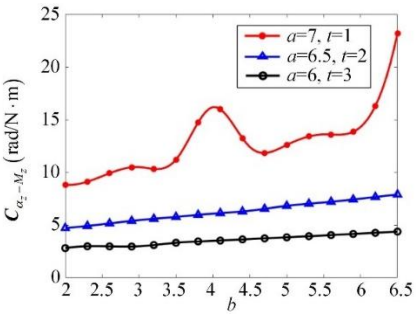

c

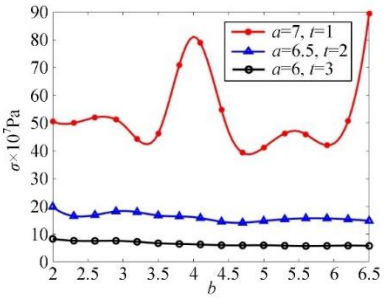

d

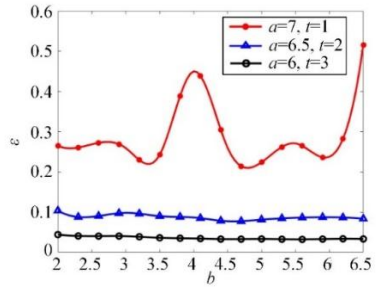

e

Fig. 10 The influence of parameters *b* on compliance, stress and strain: a – compliance C_{x-F_x}, b – compliance C_{y-F_y}, c – compliance $C_{\alpha_z-M_z}$, d – stress, e – strain

fluence of n on compliance, stress, and strain is more pronounced compared to r. Among the various compliance, C_{y-F_y} attains its maximum value within the range of n and r, while $C_{\alpha_z-M_z}$ achieves its minimum value. When r is at its minimum and n is at its maximum, all compliances, stresses, and strains reach their minimum values.

For 3-RRR flexible linkage mechanism with circular flexure hinges, as the radius r of the circular arc varies, the minimum thickness t correspondingly adjusts, r and t are variables that vary within their ranges $r \in [4.75, 7]$, $t \in [1, 5.5]$. The relationships between the compliance, stress and strain of the circular flexure hinge and the parameters of notch sizes r and t were analyzed using ANSYS and MATLAB, as illustrated in Fig. 8, a-e.

As illustrated in Fig. 8, a-e, an increase in the arc radius r results in a nonlinear increase in compliance, stress, and strain. Conversely, an increase in the minimum thickness t leads to a nonlinear decrease in compliance, stress and strain. The effect of r on these parameters is more pronounced compared to that of t. Within the range of values for r and t, the compliance exhibits both a maximum and a minimum value. Specifically, when r is at its minimum and t is at its maximum, the compliance, stress and strain all attain their minimum values.

For 3-RRR flexible linkage mechanism with elliptical arc flexure hinges, When the minor semi-axis b is held constant, the major semi-axis a and the minimum thickness t serve as variables, varying within their ranges $\alpha \in [4.75, 7]$, $t \in [1, 5.5]$. The relationships between the compliance, stress, and strain of the elliptical arc flexure hinge and the parameters of notch sizes a and t are obtained using Ansys and MATLAB, as shown in Fig. 9, a-e. From Fig. 9, a-e, several characteristics can be observed, as described below.

As illustrated in Fig. 9, a-e, an increase in the major semi-axis a result in a nonlinear increase in compliance, stress and strain. Conversely, an increase in the minimum thickness t leads to a nonlinear decrease in compliance, stress and strain. The effect of a on these parameters is more pronounced compared to that of t. Within the range of values for a and t, the compliance exhibits both a maximum and a minimum value. Specifically, when a is at its minimum and t is at its maximum, the compliance, stress and strain all attain their respective minimum values.

When the major semi-axis a and the minimum thickness t are held constant while the minor semi-axis b varies, varying within ranges of $b \in [2, 6.5]$. Three distinct combinations of values are selected for the major semi-axis a and the minimum thickness t. The relationships between the compliance, stress and strain of the elliptical arc flexure hinge and the parameters of notch sizes b are plotted using Ansys and MATLAB's cubic spline interpolation function, as shown in Fig. 10, a-e. From Fig. 10, a-e, several characteristics can be observed, as described below.

5. Conclusions

In summary, this study developed a 3-RRR flexible gripping mechanism utilizing notched flexure hinges as bionic joints. The analytical formula for the output compliance of the notched flexure hinge-based bionic joint flexible linkage mechanism was derived and validated, with an error controlled within approximately 8%. The primary contribution of this research lies in analysing the influence of different notch shapes and dimensions of flexure hinges on the performance of the flexible linkage mechanism. a comprehensive comparison of the compliance performance and stress-strain characteristics among U-shaped, circular arc-shaped, and elliptical arc-shaped notches revealed significant differences. The compliance of the U-shaped notch flexure hinge is slightly lower than that of the circular arc-shaped notch flexure hinge, with their values being relatively close. However, the compliance of the U-shaped notch flexure hinge is significantly higher than that of the elliptical arc-shaped notch flexure hinge. In terms of stress-strain characteristics, the U-shaped notch flexure hinge exhibits the smallest stress and strain, followed by the circular arc-shaped notch flexure hinge, while the elliptical arc-shaped notch flexure hinge demonstrates the largest stress and strain. Overall, the U-shaped notch flexure hinge demonstrates superior comprehensive performance compared to the other two types. Therefore, when employed as a bionic joint in the 3-RRR flexible mechanism, the U-shaped notch flexure hinge offers excellent compliance while maintaining lower stress and strain levels. Among the dimensional parameters of the U-shaped notch flexure hinge (n, r, and t), the straight notch depth n has the most substantial impact on the performance of the flexible linkage, while the minimum thickness t has the least influence. For the circular arc-shaped notch flexure hinge, the arc radius r affects the performance of the flexible linkage more significantly than thickness t. Among the dimensional parameters of the elliptical arc-shaped notch flexure hinge (a, b, and t), the semi-major axis a has a more pronounced impact on the performance. The findings of this study provide practical theoretical value for the design and application of bionic joints in flexible mechanisms. Although this study has certain limitations, primarily focusing on static compliance performance and stress-strain analysis, the use of a large number of analytical models (80 sets) effectively elucidates the influence of notch shape and parameters on performance.

This study confirms that the U-shaped notch flexible hinge, when employed as a bionic joint in a 3-RRR compliant linkage, achieves an ideal combination of high compliance and low stress levels. This characteristic has profound implications for its performance in practical applications: In terms of strength, the low peak stress ensures a higher safety margin for the hinge when bearing both operational loads and unexpected overloads. Its superior compliance is realized without compromising the overall structural robustness. Regarding durability under low-cycle operation, the low strain amplitude is the cornerstone of long service life. Combined with its smooth geometric transition, the hinge exhibits excellent damage tolerance and structural resilience, enabling reliable performance under large-deformation cyclic loading and effectively resisting permanent damage. For high-cycle operational durability, the low working stress implies that its alternating stress amplitude is expected to fall below the material's fatigue limit. This opens the possibility for achieving an 'infinite life' design, particularly suitable for automation scenarios requiring long-term, high-frequency operation.

Acknowledgements

This research was supported by the Central Government Guiding Local Science and Technology Development Fund (Grant No: YDZJSX2024D079), the Foundation of Shanxi Key Laboratory of Advanced Manufacturing Technology (Grant No. XJZZ202306).

References

1. **Yu J. J.; Pei, X.; Bi, S. S.; Zong, G. H.; Zhang, X. M.** 2010. State-of-arts of Design Method for Flexure Mechanisms. Journal of Mechanical Engineering 46(13): 2–12.
2. **Yu, J. J.; Hao, G. B.; Chen, G. M.; Bi, S. S.** 2015. State-of-art of Compliant Mechanisms and Their Applications, Journal of Mechanical Engineering 51(13): 53-68.
3. **Tian, Y.; Shirinzadeh, B.; Zhang, D.; Zhong, Y.** 2010. Three flexure hinges for compliant mechanism designs based on dimensionless graph analysis, Precision Engineering 34(1): 92-100. https://doi.org/10.1016/j.precisioneng.2009.03.004.
4. **Lobontiu, N.** 2014. Compliance-based matrix method for modeling the quasi-static response of planar serial flexure-hinge mechanisms, Precision Engineering 38(3): 639-650. https://doi.org/10.1016/j.precisioneng.2014.02.014.
5. **Rus, D.; Tolley, M. T.** 2015. Design, fabrication and control of soft robots, Nature 521(7553): 467-475. https://doi.org/10.1038/nature14543.
6. **Wang, T. M.; Meng, C.; Guan S. G.; Pei, B. Q.** 2009. Structure Design of Gecko Robot with Compliant Shank, Journal of Mechanical Engineering 45(10): 1-7. Available at: http://www.cjmenet.com.cn/EN/Y2009/V45/I10/1.
7. **Li, Y.; Ge, W. J.; Kou, X.** 2013. Research and design on foot of hopping kangaroo robot based on compliant mechanisms, Journal of Machine Design 30(2): 18-24 (in Chinese). http://doi.org/10.13841/j.cnki.jxsj.2013.02.008.
8. **Pang, Z. X.; Wang, T. Y.; Yu, J. Z.; Liu, S.; Zhang, X. Y.; Jiang, D. W.** 2020. Design and Analysis of a Flexible, Elastic, and Rope-Driven Parallel Mechanism for Wrist Rehabilitation, Applied Bionics and Biomechanics 2020: 8841400. http://doi.org/10.1155/2020/8841400.
9. **Wang, C. D.; Wang, L.; Wang, T. H.; Li, H. P.; Du, W. L.; Meng, F. N.; Zhang, W. W.** 2019. Research on an Ankle Joint Auxiliary Rehabilitation Robot with a Rigid-Flexible Hybrid Drive Based on a 2-S'PS' Mechanism, Applied Bionics and Biomechanics 2019: 7071064. http://doi.org/10.1155/2019/7071064.
10. **Wei, D. W.; Gao, T.; Mo, X. J.; Xi, R. R; Zhou, C.** 2020. Flexible Bio-tensegrity Manipulator with Multi-degree of Freedom and Variable Structure, Chinese Journal of Mechanical Engineering 33(1): 3. http://doi.org/10.1186/s10033-019-0426-7.
11. **Xi, H. Y.; Wang, T.; Yao, C.; Xu, Y.; Li, X. F.** 2019. Research on bionic soft gripper drive by motor, Chinese High Technology Letters 29(4): 362-370 (in Chinese). http://doi.org/10.3772/j.issn.1002-0470.2019.04.007.
12. **Yu, Y. Q.; Ma, L.; Cui, Z. W.; Li, Y.** 2014. Design and Experiment of Open Thin-walled Flexure Joints of Parallel Robot, Transactions of the Chinese Society for Agricultural Machinery 45(5): 284-290 (in Chinese). http://doi.org/10.6041/j.issn.1000-1298.2014.05.044.
13. **Meng, Q. L.; Shen, Z. J.; Chen, Z. Z.; Nie, Z. Y.** 2020. Design and Research of Bionic Hand Exoskeleton Based on Flexible Hinge, Chinese Journal of Biomedical Engineering 39(5): 557-565 (in Chinese). http://doi.org/10.3969/j.issn.0258-8021.2020.05.006.
14. **Ma, T. Yang, D.; Zhao, H. W.; Li, T.; Ai, N.** 2020. Grasping Analysis and Optimal Design of a Novel Underactuated Robotic Gripper, Robot 42(03): 354-364. (in Chinese). http://doi.org/10.13973/j.cnki.robot.190412.
15. **Wang, Z. F.** 2019. Research on the design of flexible mechanical finger based on the analysis of hand grasping behavior. South China University of Technology (in Chinese). http://doi.org/10.27151/d.cnki.ghnlu.2019.001972.
16. **Zhou, J. S.; Chen, S.; Wang, Z.** 2017. A Soft-Robotic Gripper With Enhanced Object Adaptation and Grasping Reliability, IEEE Robotics and Automation Letters 2(4): 2287-2293. http://doi.org/10.1109/LRA.2017.2716445.
17. **Liu, X. M.; Wang, Y. Q.; Geng, D. X.; Zhao, Y. W.; Zhang, J. T.** 2012. Dynamics Investigation on Bidirectional Active Flexible Bending Joints, Advanced Materials Research 422: 529-533. https://doi.org/10.4028/www.scientific.net/AMR.422.529.
18. **Wu, Z. P.; Li, X. N.; Guo, Z. H.** 2019. A Novel Pneumatic Soft Gripper with a Jointed Endoskeleton Structure, Chinese Journal of Mechanical Engineering 32(1): 78. http://doi.org/10.1186/s10033-019-0392-0.
19. **Alici, G.; Canty, T.; Mutlu, R.; Hu, W. P.; Secadas, V.** 2018. Modeling and Experimental Evaluation of Bending Behavior of Soft Pneumatic Actuators Made of Discrete Actuation Chambers, Soft Robotics 5(1): 24-35. http://doi.org/10.1089/soro.2016.0052.
20. **Abondance, S.; Teeple, C. B.; Wood, R. J.** 2020. A Dexterous Soft Robotic Hand for Delicate In-Hand Manipulation, IEEE Robotics and Automation Letters 5(4): 5502-5509. http://doi.org/10.1109/LRA.2020.3007411.
21. **Sinatra, N. R.; Teeple, C. B.; Vogt, D. M.; Parker, K. K.; Gruber, D. F.; Wood, R. J.** 2019. Ultragentle manipulation of delicate structures using a soft robotic gripper, Science Robotics 4(33): 1-11. http://doi.org/10.1126/scirobotics.aax5425.
22. **Friedrich, R.; Lammering, R.; Rösner, M.** 2014. On the modeling of flexure hinge mechanisms with finite beam elements of variable cross section, Precision Engineering 38(4): 915-920. http://doi.org/10.1016/j.precisioneng.2014.06.001.

J. Liang, R. Li, W. Guo, L. Zhang, Q. Zhang

MECHANICAL BEHAVIOR ANALYSIS OF BIO-INSPIRED JOINTS WITH NOTCHED FLEXURE HINGES

S u m m a r y

This study derives the analytical calculation formula for the output compliance of a notched flexure hinge-based bio-inspired joint linkage mechanism in flexible gripping mechanism. Finite element analysis (FEA) was conducted to investigate the compliance characteristics of three distinct notch-type 3-RRR flexible link. The correctness of the analytical solution was validated by comparing it with the finite element solution. Further investigation into the influence of structural parameters on the performance characteristics of 3-RRR flexible link was conducted, establishing correlation curves between geometric parameters and both compliance and stress-strain characteristics. Through comprehensive comparison, the notch configuration demonstrating optimal overall performance in 3-RRR flexible link was identified.

Keywords: flexible gripping mechanism, notched flexure hinge, bio-inspired joint, 3-RRR flexible link.

Received June 4, 2025
Accepted October 22, 2025